UC San Diego

Title

Effective treatment of retinal neovascular leakage with fusogenic porous silicon nanoparticles delivering VEGF-siRNA

Permalink

https://escholarship.org/uc/item/2t94r22k

Journal

ISSN

Authors

Grondek, Joel F
Huffman, Kristyn
Lee, Ella Jiyoon
et al.

Publication Date

DOI

Peer reviewed

Nanomedicine

Effective treatment of retinal neovascular leakage with fusogenic porous silicon nanoparticles delivering VEGF-siRNA

Joel F Grondek*,1 [iD], Kristyn Huffman2, Ella Jiyoon Lee1, Melina Cavichini2, Alexandra Warter2, Fritz Gerald P Kalaw2, Anna Heinke2, Ruhan Fan3, Lingyun Cheng2, Michael J Sailor1,3 & William R Freeman2

1Department of Chemistry & Biochemistry, University of California, San Diego, CA 92093, USA
2Department of Ophthalmology, Jacobs Retinal Center at Shiley Eye Institute, University of California, San Diego, CA 92093, USA
3Materials Science & Engineering, University of California, San Diego, CA 92093, USA
*Author for correspondence: jgrondek@ucsd.edu

Aim: To evaluate an intravitreally injected nanoparticle platform designed to deliver VEGF-A siRNA to inhibit retinal neovascular leakage as a new treatment for proliferative diabetic retinopathy and diabetic macular edema. **Materials & methods:** Fusogenic lipid-coated porous silicon nanoparticles loaded with VEGF-A siRNA, and pendant neovascular integrin-homing iRGD, were evaluated for efficacy by intravitreal injection in a rabbit model of retinal neovascularization. **Results:** For 12 weeks post-treatment, a reduction in vascular leakage was observed for treated diseased eyes versus control eyes (p = 0.0137), with a corresponding reduction in vitreous VEGF-A. **Conclusion:** Fusogenic lipid-coated porous silicon nanoparticles siRNA delivery provides persistent knockdown of VEGF-A and reduced leakage in a rabbit model of retinal neovascularization as a potential new intraocular therapeutic.

Diabetic retinopathy is a leading cause of blindness in the industrialized world, with a global prevalence of an estimated 95 million people [1]. Administration of anti-VEGF therapies is the standard of care for the treatment of proliferative diabetic retinopathy (PDR) and diabetic macular edema (DME) [2,3]. In 2015, there were over 2.6 million anti-VEGF injections in the USA [4], with a conservative estimate of 3.6 million annual injections by 2023. The chronic pathology of the disease requires a protracted level of therapeutic intervention to maintain remission. Due to the high turnover of anti-VEGF in the vitreous, repeated monthly injections are required [5–9]. In the Horizon study of community-based anti-VEGF injections in wet age-related macular degeneration (AMD), the vision gain attained from repeated 4-week injections of the anti-VEGF drug ranibizumab was lost once the patients transitioned to an as-needed regimen [10]. This result was also seen in the seven-year outcomes follow-up study of ranibizumab [11]. However, continued, repeat intravitreal injections run the risk of intraocular inflammation, infection and ocular hemorrhage [12]. Bolus high-dose intravitreal injection can result in adverse reactions from systemic circulation [13]. There are similar issues in PDR, where premature discontinuation of anti-VEGF may result in the resurgence of the disease [14]. To treat or prevent PDR, it has been suggested that anti-VEGF drugs be used chronically and that they likely produce less retinal damage than panretinal photocoagulation therapy [15]. Monthly injections, however, are not practical for many and more permanent or long-acting treatment is desired. An alternative approach is to use RNA interference to silence VEGF mRNA expression.

siRNA therapeutics have a catalytic advantage over their antibody-based counterparts. Once the siRNA-RNA-induced silencing complex forms it can cleave multiple VEGF messenger RNAs, as opposed to anti-VEGF which stoichiometrically sequesters VEGF protein [16]. Approximately 10 years ago, phase III clinical trials tested the free drug VEGF-siRNA bevasiranib in combination with the anti-VEGF drug ranibizumab to treat neovascularization-linked AMD [17]. The results of this study suggested that free siRNA is efficacious in inhibiting neovasculariza-

tion; however, the combination therapy did not outperform ranibizumab alone [17]. In addition, while bevasiranib was being evaluated for clinical use, other researchers demonstrated that extracellular VEGF-siRNA can indiscriminately arrest AMD neovascularization by binding the extracellular TLR3, in lieu of its intracellular target VEGF mRNA, and can induce apoptosis [18,19]. Subsequent years have seen many advances in the development of siRNA as a therapeutic. There are currently three US FDA-approved siRNA therapeutics, nine in phase III clinical trials and thirteen in phase II clinical trials (clinicaltrials.gov). One key factor leading to the surge of recent clinical activity is the substantially greater stability of the latest siRNA constructs. This enhanced stability is provided by a number of specific modifications on individual ribose sugars, which reduce the susceptibility to nuclease cleavage and enhance gene knockdown [20]. While these modifications have increased the *in vivo* half-life of siRNAs by over three orders of magnitude [21], an obstacle for intraocular applications of siRNA therapy remains: how to effectively deliver functional siRNA through the vitreous to target the diseased retinal cells. We hypothesized that these obstacles could be overcome by utilizing recent advances in nanomedicine, in particular: 1) nanoparticles with the ability to carry high quantities of siRNA, 2) peptides capable of selectively targeting and penetrating cells and 3) fusogenic coatings that avoid endosomal uptake to enhance cytosolic delivery.

The nanoparticle system chosen for this study was composed of mesoporous silicon, a material that has been shown to be well-tolerated by tissues of the eye [22–26] and that can protect the siRNA payload from RNase degradation [27]. Nucleic acid therapeutics such as siRNA possess a high negative charge due to their phosphate backbone, and generally this charge must be neutralized in order for sufficient quantities to be loaded into a nanoparticle. While surface modification with a positively charged species such as cationic lipids or polymers is a common solution that has also been used for silicon nanoparticles [28–32], for this work a biocompatible calcium-silicate condenser chemistry was used. When applied to porous silicon nanoparticles (pSiNPs), this chemistry has been shown to yield mass loadings of nucleic acid in excess of 20% [33,34] and to prolong delivery of the siRNA payload [33] while retaining the ability of nanophase silicon to dissolve into harmless byproducts *in vivo* [26]. To bypass endosomal uptake/degradation, the pSiNPs were coated with a fusogenic lipid coating to make fusogenic lipid-coated pSiNPs (F-pSiNPs) [34–36]. We chose to target retinal angiogenesis using the tumor-homing and internalization peptide iRGD which has been widely studied and shown to penetrate deep into tumor vasculature [37–40]. Like its progenitor, the RGD peptide, iRGD targets cell surface αv integrins via the RGD peptide sequence. The i-prefix on iRGD indicates 'internalizing', and this relates to the affinity of the RGDK sequence in iRGD for the cell surface receptor neuropilin-1, which enables cellular internalization [37–40]. Both αv integrins and neuropilin-1 are known to be expressed on the surface of cells associated with choroidal neovascularization [41,42], although their upregulation in retinal angiogenesis is not known. This study sought to test the ability of this targeted nanocarrier system to deliver VEGF-siRNA within the retina.

The *in vivo* rabbit model was chosen for retinal neovascularization and vascular leakage indicative of pathologic vessel growth associated with PDR. The Müller cell toxin DL-a-aminoadipic acid (DL-AAA) is injected intravitreally and has been shown to induce the pathology of the model within 2 weeks of injection [43–45]. Müller glial cells are specific to the retina and are responsible for protecting neurons, maintaining homeostasis and neuronal metabolic support [46]. They have been shown to undergo gliosis in PDR and, in doing so, contribute to the progression of the disease by the release of angiogenic cytokines such as VEGF [46,47]. VEGF, in turn, promotes neovascular growth and induces vascular leakage [2,3]. A single injection of DL-AAA exhibited a neovascular retinal pathology in rabbits from 2 to 65 weeks postinjection [43,44]. This DL-AAA rabbit model of retinal neovascularization presents vascular leakage that can be readily monitored by fluorescein angiography (FA), and its relevance to the disease pathology has been validated by demonstration of attenuation of FA leakage upon injection of the anti-VEGF drug aflibercept [43,44].

In this study, we loaded pSiNPs with rabbit VEGF-siRNA using the above calcium silicate condensation chemistry, then applied the fusogenic lipid coating and conjugated iRGD to the exterior of the nanoparticle via a 2 kDa PEG-maleimide linker. To test the efficacy of the resulting VEGF-siRNA F-pSiNPs by single intravitreal injection, we monitored the DL-AAA rabbit model over a 12-week period by FA, VEGF assays of vitreous eye taps and histology. To our knowledge, this is the first demonstration of intravitreal delivery of siRNA utilizing iRGD to successfully treat an animal model of retinal neovascularization.

Materials & methods

Materials

Highly boron-doped p++ type silicon wafers, ~1 mΩ cm resistivity, polished on the (100) face (Sil'tronix, Inc., Archamps, France); hydrofluoric acid, 48% aqueous, American Chemical Society Grade (ACS; Thermo Fisher Scientific Inc., MA, USA); anhydrous calcium chloride (Spectrum Chemicals, NJ, USA); 1,2-dimyristoyl-sn-glycero-3-phosphocholine (DMPC), 1,2-dioleoyl-3-trimethylammonium-propane (DOTAP) and 1,2-distearoyl-sn-glycero-3-phosphoethanolamine-N-(maleimide[PEG]-2000) (DSPE-PEG-maleimide; Avanti Polar Lipids, AL, USA); 1,1′-dioctadecyl-3,3,3′,3′-tetramethylindocarbocyanine perchlorate (DiI) and Lipofectamine 2000 (Thermo Fisher Scientific Inc.); iRGD peptide: 5FAM-C[X]CRGDKGPDC-NH2 and control peptide: 5FAM-C(X)CRGEDGPKC (AnaSpec, CA, USA), where (X) = 6-amino hexanoic acid; s-s bonds between C3 and C11; rabbit VEGF-A siRNA [48] was modified with the addition of 2′ methoxy to the first two 5′ nucleosides of the antisense strand: 5′mA.mU.G.U.C.C.A.C.C.A.A.G.G.U.C.U.C.G.A.dT.dT3′; sense: 5′U.C.G.A.G.A.C.C.U.U.G.G.U.G.G.A.C.A.U.dT.dT3′; both with and without 5′-Cy5.5 fluorophore on the sense strand (Horizon-Dharmacon Inc., IL, USA); human ARPE-19 cells (American Type Culture Collection, www.atcc.org); rabbit VEGF-A ELISA kit and human VEGF-A ELISA kit (MyBioSource, CA, USA); M-PER mammalian protein extraction reagent (Thermo Fisher Scientific Inc.); rabbit antiglutamine synthetase AF488 MBS8577666 (MyBioSource); New Zealand pigmented rabbits (males and females), 3–4 months old (Western Oregon Rabbitry, OR, USA); balanced salt solution (BSS) and DL-AAA (MilliporeSigma, MA, USA); and Toxin-Sensor Chromogenic LAL Endotoxin Assay Kit (GenScript, NJ, USA).

Preparation of F-pSiNPs

The F-pSiNPs were synthesized as previously described [35]. Porous silicon (pSi) was produced by electrochemical anodization of highly boron-doped p++ type silicon wafers (exposed area ~9 cm^2) using a square waveform with a current density of 50 mA cm^{-2} applied for 0.6 s followed by a current density 400 mA cm^{-2} for 0.36 s, repeated for 500 cycles in 3:1 aqueous 48% HF:absolute ethanol (CAUTION: HF is highly toxic and proper care should be exerted to avoid contact with skin or lungs). The porous layer was removed with a current density pulse of 3.7 mA cm^{-2} for 250 s in 1:20 aqueous 48% HF:absolute ethanol, and ultrasonicated in an Avantor VWR 50T ultrasonic bath in 2 ml of water for 16 h to generate pSiNPs, and further purified by centrifugation [35]. Using aseptic technique, 150 μl of 1 mg ml^{-1} pSiNPs was mixed with 150 μl of 150 nM siRNA on ice and placed in an ultrasonic bath at ~4–6°C. A total of 700 μl of 2 M calcium chloride was added, and the mixture was ultrasonicated for an additional 15 min. The resulting particles were pelleted at 5000 × g at 4°C for 10 min. The supernatant was removed and assayed by absorbance for siRNA loading. The particles were resuspended in 1 ml of BSS, briefly ultrasonicated into solution and transferred for lipid coating. The fusogenic coating was prepared by adding DOTAP:DMPC:DSPE-PEG-2000-malemide at a mole ratio of 20:76:4, respectively. The lipids were mixed by adding 19.6 μl DOTAP, 72.6 μl DMPC, 10 mg ml^{-1} stock solutions and 15.2 μl DSPE-PEG-2000-malemide from a 25 mg ml^{-1} stock solution in chloroform and dried overnight (20 μl of the membrane dye DiI, 1.25 mg ml^{-1} in ethanol, was added to the lipid mixture for the histology and *in vitro* imaging studies). The siRNA-loaded pSiNPs were added to the dried lipids and heated to 40–45°C while stirring. The particles were extruded through a 0.2 μm membrane 20 times at 40–45°C. Then, 100 μl of the iRGD or control peptide at 1 mg ml^{-1} was added and stored at 4°C for 16 h to affect thiol-maleimide coupling. The resulting particles were washed with BSS using 30 kDa cutoff Amicon Ultracel centrifuge filter at 4500 × g for 30 min three times to a final volume less than 200 μl. The flowthrough was saved and assayed by absorbance for siRNA loading. The final particle volume was adjusted to equal 500 μg ml^{-1} siRNA based on encapsulation efficiency. Particle morphology and charge were analyzed with dynamic light scattering (DLS) using a Zetasizer and FEI Spirit transmission electron microscope (TEM).

Cryogenic electron microscopy

Cryogenic electron microscopy (Cryo-EM) and electron energy loss spectroscopy were performed on a Titan Krios G3 microscope with an extreme field emission gun (X-FEG; Thermo Fisher Scientific, Inc.) electron source operating at 300 kV, equipped with Gatan's 1067HD BioContinuum HD Imaging Filter and Gatan's K3 direct electron detector camera. Samples were prepared on Quantifoil R2/2 300 mesh copper grids prepared using Gatan's Solarus II plasma cleaner. A total of 3.5 μl of the sample was aliquoted onto the grid and plunge frozen in the Vitrobot Mark IV at 4°C and 100% humidity. Micrographs were recorded and aligned using Gatan Digital Micrograph 3.5 at a nominal magnification of 42,000× with a calibrated pixel size of 2.12 Å and the energy slit

width set to 10 eV. For electron energy loss spectroscopy, we used the scanning transmission electron microscopy mode on the Titan Krios G3 to focus the probe on specific parts of the sample to collect the spectra at an energy shift of 99.2 eV, which corresponds to silicon dioxide's $L_{2,3}$ edge.

In vitro release

In vitro release was performed by incubating the siRNA-loaded F-pSiNPs in 500 μl phosphate-buffered saline (PBS) (pH 7.4) at 500 μg ml^{-1} or 1 mg ml^{-1} at 37°C in an orbital shaker. The particles were transferred to a 30 kDa molecular weight cutoff Amicon Ultracel centrifuge filter and centrifuged at 4500 × g for 30 min. The flowthrough was measured for both volume by mass (assuming 1 g = 1 ml) and for siRNA, absorbance using a Thermo Fisher NanoDrop. The remaining particles were resuspended with PBS buffer and returned to 37°C shaking until the next time point.

In vitro cell imaging

Human retinal pigmented epithelial cells (ARPE-19) were grown to 50% confluency in growth media (GM) consisting of DMEM-F12, 10% fetal bovine serum and 1% penicillin/streptomycin to a density of 150,000 cells per mL^{-1} in a six-well plate at 37°C, 5% CO_2. All nanoparticles were incubated with cells at confluency for 20 min at 37°C followed by three equal-volume washes with GM, the addition of 0.4% paraformaldehyde diluted in GM, then 4% paraformaldehyde for 10 min, followed by two washes with Dulbecco's PBS (DPBS), subsequent 4′,6-diamidino-2-phenylindole (DAPI) staining and two final washes with DPBS. The cells were covered in DPBS and imaged within 2 h. Cells were imaged using a Nikon A1R Confocal STORM super-resolution system.

In vitro ELISA

ARPE-19 cells were grown to 80% confluency in GM to a density of 100,000 cells per mL^{-1} in a 12-well plate at 37°C, 5% CO_2. The addition of 20 μl of F-pSiNPs, or control peptide F-pSiNPs, were added per well, at a final concentration of 60 pmol siRNA each, and tested against 60 pmol of siRNA combined with Lipofectamine 2000 according to the manufacturer's protocol (n = 3 each). The culture plates were gently mixed after each addition, and incubated with cells for 24 h at 37°C. GM was replaced, and the cells were grown for an additional 24 h. GM was removed, and the cells were lysed by the addition of 400 μl M-PER (Thermo Fisher Scientific Inc., IL, USA) mammalian protein extraction reagent, shaking at 100 r.p.m. for 10 min at room temperature. The samples were then centrifuged at 14,000 × g for 10 min. The supernatants were flash-frozen in liquid nitrogen, stored at -80°C and thawed just before use. Human VEGF-A concentrations were determined by human-specific 96-well VEGF-A ELISA. The absorbance was read at 450 nm on a SpectraMax iD5 plate reader.

Flow cytometry

ARPE-19 cells were grown to 50% confluency in GM to a density of 150,000 cells per mL^{-1} in a six-well plate at 37°C, 5% CO_2. The GM was aspirated, followed by the addition of 3 ml fresh GM and 15 μl of F-pSiNPs, or control peptide F-pSiNPs, per well at 25 μg of siRNA in 50 μl (0.5 mg ml^{-1}), followed by gentle swirling of the plate and incubation at 37°C for 15 min. After incubation, the GM was aspirated, and the cells were rinsed with DPBS and collected by trypsin digestion. The cells were resuspended in DPBS with 2% fetal bovine serum (FBS) to a final concentration of 100k cells ml^{-1}. DAPI was added to 0.1 μg ml^{-1} for each sample and a cell-only control for live/dead calibration, excluding the cell-only and Cy5.5 siRNA fluorescence controls. Free Cy5.5 siRNA was added to a cell-only sample at 50 μg ml^{-1} for fluorescence calibration control. All assays were prepared at n = 3. A BD FACSCalibur, four-color, dual-laser benchtop flow cytometer was used for the analysis.

Animal studies

All animal studies were performed using New Zealand pigmented rabbits, which were treated in accordance with the University of California San Diego, Institutional Animal Care and Use Committee (IACUC) standards of practice and the Association for Research in Vision and Ophthalmology statement for the use of animals in ophthalmic and vision research. Intraocular injections, FA, electroretinogram (ERG) and optical coherence tomography (OCT) were performed under 25–30 mg/kg ketamine and 5 mg/kg xylazine administered by subcutaneous injection. For intraocular injections, the eye was surgically prepped with ophthalmic betadine, then sterilely irrigated with BSS. Then one to two drops of proparacaine were administered to numb the cornea. All intraocular injections were performed under an Alcon ophthalmic operating microscope.

Table 1. Summary of *in vivo* intravitreal rabbit studies.						
Study	Time frame	Animals (n)	Eye	DL-α-aminoadipic acid (injected)	Treatment	
					VEGF-siRNA-loaded fusogenic porous silicon nanoparticles	Balanced salt solution
Histology	72 h post-treatment	2	OD	+	+	–
			OS	–	–	–
Indirect fundus exam electroretinography, optical coherence tomography	At weeks 2, 4, 8 and 12 post-treatment	4	OD	–	+	–
			OS	–	–	–
Indirect fundus exam fluorescein angiography	At week 0 and every 2 weeks post-treatment for 12 weeks	5	OD	+	+	–
			OS	–	–	–
		4	OD	+	–	+
			OS	–	–	–
Vitreous ELISA	1-week post-treatment	4	OD	+	+	–
			OS	–	–	–
		4	OD	+	–	+
			OS	–	–	–
	4-weeks post-treatment	4	OD	+	+	–
			OS	–	–	–
		4	OD	+	–	+
			OS	–	–	–
	12-weeks post-treatment	4	OD	+	+	–
			OS	–	–	–
		3	OD	+	–	+
			OS	–	–	–
		38	= total number of study animals			

(+) received injection, (-) no injection.
Studies on New Zealand pigmented rabbits of mixed gender.
OD: Right eye; OS: Left eye.

Toxicity & inflammation

A total of 50 µl of F-pSiNPs-iRGD containing a total of 25 µg of VEGF-A siRNA was injected into the right eye of four healthy New Zealand pigmented rabbits, and their fellow eye was left as a noninjection control (Table 1). At weeks 2, 4, 8 and 12 postinjection, the animals' retinas were measured for functional changes by ERG, imaged by OCT, and viewed by clinically trained ophthalmologists by fundus exam and assessed for inflammation and toxicity. ERG measurements were performed as previously described [49]. In brief, eyes were given one to two drops of proparacaine, dilated with 2.5% phenylephrine-HCl and 1% tropicamide, and dark-adapted for 30 min. The rabbits were anesthetized as described above. Responses were obtained from the cornea using Jet-electrode contact lenses (LKC Technologies). Low- and high-frequency cutoffs were set to 0.3 Hz and 500 Hz. The illuminance on the surface of the eye was approximately 2.8 lux for light intensity designated I, less the reduction by neutral density filters ND2 and ND1. The duration of the flash was 10 µsec. ERGs of five stimuli were averaged over a response window of 500 msec. The b-wave amplitude was measured from the trough of the a-wave to the peak of the b-wave and was compared between the eyes with F-pSiNPs and normal contralateral control eyes, pooled. OCT images were obtained using a Heidelberg SD-OCT/SLO Spectralis imaging system with seven slices through both nasal and temporal regions, inferior to the optic nerve. OCT images were assessed by clinically trained ophthalmologists for retinal toxicity/inflammation.

DL-AAA model

A total of 80 µl of an 80 mM DL-a-aminoadipic acid (DL-AAA) solution was injected into one eye of a rabbit to initiate the retinal neovascularization model, as previously described [43,44]. The contralateral eye was injected with 80 µl BSS as a control. The DL-AAA solution was prepared on the day of use under sterile conditions by dissolving 128.9 mg of DL-AAA in 1 ml 1 M HCl, diluted with BSS to a final volume of 10 ml, pH adjusted to 7.4 with 2 M NaOH and filtered with 0.22 µm syringe filter. Of these animals, five were used for our treatment and four as

controls (Table 1). DL-AAA eyes that resulted in partial retinal detachment at 2 weeks postdisease induction were excluded from the FA study because the leakage could no longer be assessed with FA imaging (∼50% of animals injected). These animals were used for analyzing nanoparticle efficacy by measuring VEGF-A from the vitreous humor, which was analyzed by ELISA for both treated and sham n = 3 or 4 each at time points of 1-, 4- and 12-weeks post-treatment (Table 1).

Nanoparticle efficacy measured by FA image analysis

The progression of the pathology was evaluated by FA at the early (0–3 min), mid (4–6 min) and late (10–13 min) phases. Then, 50 μl of F-pSiNPs-iRGD containing a total of 25 μg of VEGF-A siRNA or a BSS-only sham was injected into the disease model DL-AAA eye of a rabbit. The contralateral eye was left untreated. FA imaging was performed on anesthetized animals every 2 weeks until week 14 postdisease induction. The FA images were montaged using the 'mid' timepoint, described above, to include the optic nerve, nasal and temporal medullary rays using Heidelberg Eye Explorer imaging software. The FA images were then exported as TIFF files and analyzed using ImageJ [50] by masked ophthalmologists at each time point to determine the pathologically observable effects of neovascularization: leakage area and intensity, vessel tortuosity and intraretinal microvascular anomalies (IrMAs). The area of leakage was circled and measured for the area and mean pixel intensity. This mean pixel intensity was corrected for gain, that is, exposure, by using the mean pixel intensity within the optic nerve contained by that image. The resulting corrected intensity was multiplied by the pixel area of leakage circled to give a quantitative measure for leakage. These recorded measurements were collected from each ophthalmologist and averaged. For the final analysis, the leakage measured on the day of treatment, prior to treatment, was used as a baseline for all subsequent leakage assessments following the relationship: ([leakage timepoint - baseline leakage]/[baseline leakage] +1) × 100% = percentage of leakage increase. Retinal vessel tortuosity was graded 0–3 (0 = not tortuous; 1 = vessels reach visual streak; 2 = vessels exceed visual streak'; 3 = 2 plus neo-vessel development). IrMAs were graded 1–3 (1 = 0–25 lesions; 2 = 25–50 lesions; 3 = >50 lesions).

Ex vivo ELISA

Rabbit VEGF-A vitreous concentrations were determined by rabbit-specific 96-well VEGF-A ELISA (My-BioSource) (Table 1) at weeks 1, 4 and 12 post-treatment; see the above section titled 'DL-AAA model'. The vitreous samples were centrifuged at 10,000 × g for 10 min at 4°C, and the supernatant was tested and measured against the nondiseased control eye by direct comparison for each animal. The absorbance was read at 450 nm on a BD SpectraMax iD5 plate reader.

Histology

A total of 50 μl of F-pSiNPs-iRGD containing ∼6.2 μg of DiI and 25 μg of Cy5.5-labeled VEGF-A siRNA was injected into the right eye of two New Zealand pigmented rabbits, 2 weeks after DL-AAA injection as described above, and their fellow eye was left as a noninjection control (Table 1). At 72 h post-treatment, the animals were sacrificed, and the eyes were punched at 3 and 9 o'clock locations with a 1 mm diameter biopsy punch at a distance of 1 mm from the limbus. The eyes were placed in 25 ml 10% formalin for 72 h at 4°C, then placed in 10%, 20% and 30% sucrose at 4°C for ∼24 h each in order of increasing concentration. Finally, the eyes were bisected in the sagittal plane with a razor blade and mounted in Neg-50 Frozen Section Medium in an isobutane/dry ice bath. The eyes were sectioned at a maximum thickness of 10–12 μm and either mounted with Prolong Gold with DAPI or stained prior to mounting with rabbit antiglutamine synthetase AF-488 primary antibody as follows. The sections were removed from -80°C storage and brought to room temperature for 10 min. The sections were incubated with PBS 25°C for 10 min, followed by blocking with 1% horse serum in PBS for 30 min. The antibody was diluted 1:200 with a buffer containing 1% bovine serum albumin (BSA), 1% heat-treated normal donkey serum, 0.3% Triton X-100 and 0.01% sodium azide in PBS and incubated on the sections overnight at 4°C. The sections were washed three times, 15 min each with PBS, followed by mounting as described above. The mounted sections were allowed to dry at room temperature overnight, protected from light and stored at 4°C. Sections were imaged using the Nikon A1R Confocal STORM super-resolution system.

Statistical analysis

FA leakage data were analyzed using SAS (SAS Institute Inc.), using general linear model (GLM) repeated measures analysis of variance. ELISA data were analyzed by one-way analysis of variance. Flow cytometry data were measured using Satterthwaite t-test. ERG data were analyzed using upper and lower t-test, pooled.

Results

The pSiNPs were prepared by electrochemical etching of silicon wafers [51] (Figure 1A). The porosity, average mesopore size and average nanoparticle size are precisely controlled by the electrochemical waveform used in the synthesis [52]. This provides a systematic means to tailor the material for a specific drug molecular size, loading capacity and/or final particle diameter. To effectively protect and deliver siRNA *in vivo*, the siRNA drug payload was condensed within the pores of the nanoparticles using a calcium silicate sealant chemistry [33]. This condensation chemistry capitalizes on the unique ability of calcium ions to both stabilize siRNA via ion pairing and to form a precipitate with silicic acid [33]. The silicic acid species, primarily in the form $Si(OH)_4$, are locally generated at the surface of the oxidized pSiNPs via aqueous dissolution; reaction with excess calcium ion creates an insoluble calcium silicate phase (idealized as dicalcium orthosilicate, Ca_2SiO_4) effectively trapping the siRNA within the pores of the nanoparticle [33] (Figure 1B). The necessity of the silicic acid species to affect the sealing of the pores limits the reaction proximity to the silicon surface. Once formed, the insoluble calcium silicate sealant slows the degradation of the porous silicon particles and, thus, the release of siRNA. To avoid engaging the endocytosis pathway, which inhibits the effectiveness of siRNA, the siRNA-loaded pSiNPs were coated with a fusogenic lipid coating (to make F-pSiNPs) as previously described [34,35] and conjugated to a 5-carboxyfluorescein (5FAM)-labeled iRGD targeting peptide (Figure 1B). This combination of targeting peptide and fusogenic coating has been shown to act by first engaging the nanoparticle with the cellular surface and then fusing with the cellular membrane, at which point the lipid coating is shed, and the nanoparticle with its siRNA payload is released directly into the cytosol [35]. For the siRNA payload, rabbit VEGF-A-siRNA was used. The antisense sequence was the following: 5′mAmUGUCCACCAAGGU- CUCGAdTdT3′ [48], where the 2′ methoxy groups at the 5′ end were introduced to protect the siRNA against exonucleolytic digestion. The iRGD targeting peptide construct consisted of 5FAM-C(X)CRGDKGPDC, where 5FAM was conjugated to the N-terminus, followed by a free cysteine for nanoparticle conjugation, a hexanoic acid linker (X) and the nine-amino acid iRGD cyclized with a disulfide bond between C3 and C11. As a control, a scrambled peptide consisting of 5FAM-C(X)CRGEDGPKC was used; here, the aspartic acid from the integrin-targeting sequence RGD was substituted with glutamic acid, previously shown to inhibit targeting, and the adjacent lysine, required for neuropilin-1 internalization, was substituted with aspartic acid [40] (Figure 1C).

The F-pSiNPs had a core pSiNP diameter 68.6 +/- 10.1 nm, polydispersity index (PDI) of 0.14 +/- 0.06 and negative zeta potential of -16.4 mV +/- 0.19 measured by DLS (Figure 2A). The pSiNPs loaded with VEGF-A-siRNA and sealed with calcium silicate prior to lipid coating did not disperse well into aqueous media, and therefore reliable DLS and zeta potential data could not be obtained. The average diameter after lipid coating/extrusion, prior to peptide conjugation, was 142.2.2 +/- 16.5 nm, PDI of 0.14 +/- 0.02 and a positive zeta potential of +7.62 +/- 0.9 mV (Figure 2A). The final particle diameter, after peptide conjugation and microcentrifuge-filter purification, was 137.2 +/- 17.8 nm with PDI of 0.12 +/- 0.04 and a positive zeta potential of +17.8 +/- 1.2 mV (Figure 2A). The F-pSiNPs with scrambled control peptide had a diameter of 139.4 +/- 3.1 nm, PDI of 0.11 +/- 0.03 and positive zeta potential of +17.8 +/- 1.0 mV (Figure 2A). The F-pSiNPs had an average siRNA encapsulation efficiency of 20.3 +/- 6.4%, which corresponds to a mean mass loading of 28.8 wt.%, defined as mass of siRNA divided by the total mass of pSiNP + siRNA combined, and efficiency of conjugation of peptide to the particles was 17.3 +/- 4.3%, based on 5FAM absorbance (Figure 2B). The particle morphology was confirmed prior to lipid coating by TEM (Supplementary Figure 1A & B) and by Cryo-EM (Figure 2C) and measured by ImageJ to have a diameter of 113.9 +/- 23.8 nm. The silicon dioxide core was detected by Cryo-EM electron energy loss spectra of empty pSi microparticles (precursors to the pSiNPs) and compared with the final F-pSiNPs against previously published data for silicon dioxide [53] (Supplementary Figure 2). Endotoxin level in the final F-pSiNP formulation was 0.365 +/- 0.04 EU ml^{-1}, below the threshold for detectable ocular inflammation in rabbit vitreous of 1.0 EU ml^{-1} [54]. The particles were tested for *in vitro* release of siRNA by incubating samples containing 0.5 mg ml^{-1} and 1.0 mg ml^{-1} siRNA in PBS (pH 7.4) at 37°C in an orbital shaker. These concentrations are equivalent to 1× and 2× of the intended *in vivo* injection concentration based on the average volume of a rabbit eye of 1.5 ml. The results showed a day-1 siRNA burst release of 42% +/- 15% for 8 μg (1×) and 56%

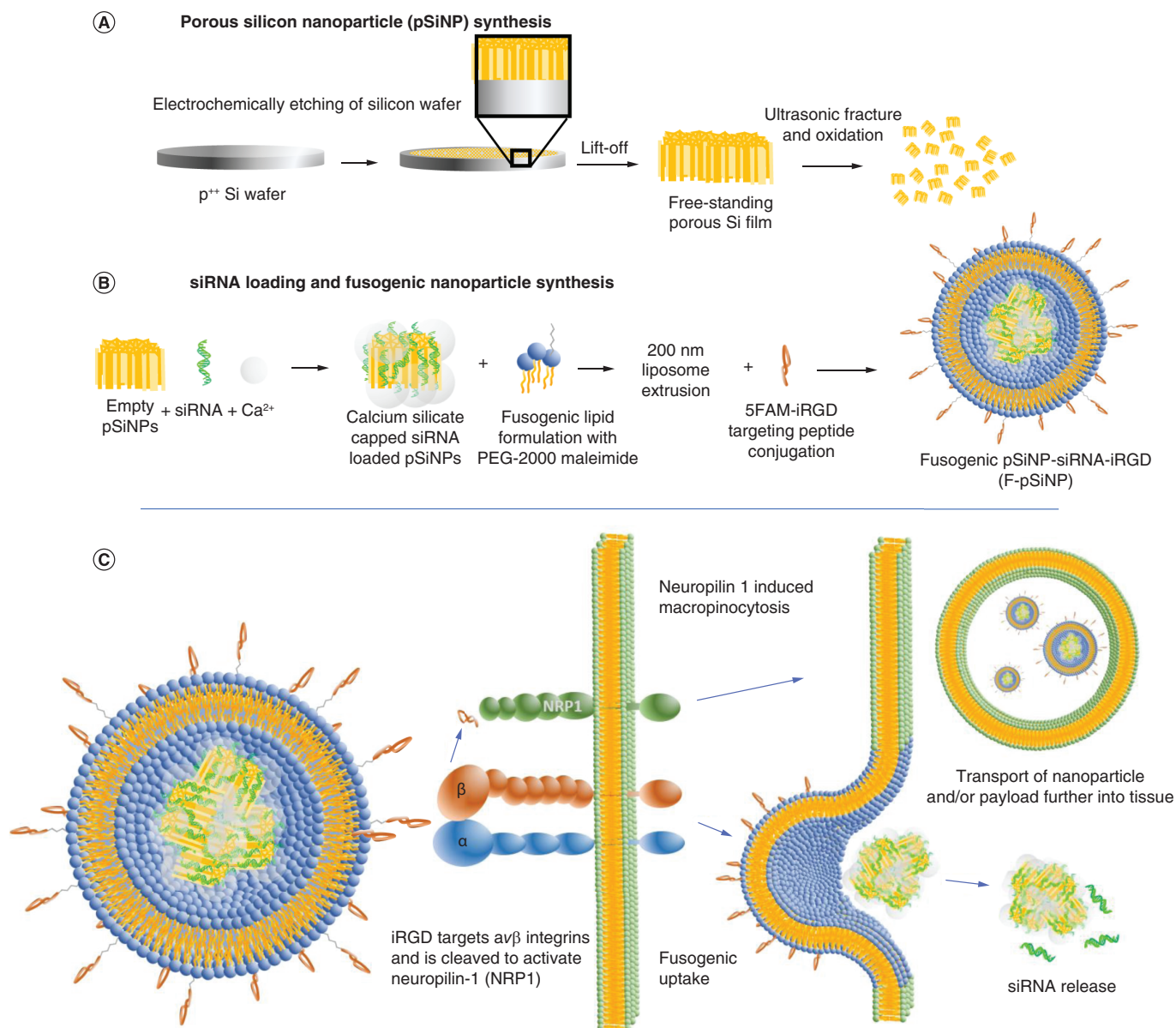**Figure 1.   The synthesis and proposed mechanism of cellular uptake of the fusogenic porous silicon nanoparticles used in this work. (A)** Electrochemical anodization of a silicon wafer selectively etches silicon to generate a nanostructured mesoporous layer which is removed and subjected to ultrasonic fracture to produce the pSiNPs. **(B)** The empty pSiNPs are loaded with a siRNA payload by means of a calcium ion-induced condensation reaction. The resulting siRNA-loaded pSiNPs are added to a fusogenic lipid mixture that also contains a PEG-2000 maleimide linker (fusogenic lipids + PEG-maleimide). Extrusion coats the solid pSiNP core with a fusogenic lipid layer. The iRGD targeting peptide (or a control peptide) is then grafted to the PEG-2000 linker via the pendant maleimide, generating the final ~150 nm nanoparticle construct (F-pSiNP-iRGD). **(C)** The iRGD targeting peptide is known to target $\alpha v \beta$ integrins at the cell surface. Once bound to the cell surface, the nanoparticle can either be directly inserted into the cytosol by fusogenic uptake, or it can be taken up by macropinocytosis after enzymatic cleavage of the peptide, which activates a neuropilin uptake pathway.
5FAM: 5-carboxyfluorescein; F-pSiNP: Fusogenic porous silicon nanoparticle; pSiNP: Porous silicon nanoparticle.

+/- 6% for 16 μg (2×), n = 4 each (Figure 2D), and essentially 100% of siRNA was released after 13 days for both concentrations tested (Figure 2E).

To test *in vitro* uptake, the F-pSiNPs were incubated with human retinal pigment epithelial cells (ARPE-19), and the uptake was assessed by confocal microscopy (Figure 3A–C). The fusogenic properties of the nanoparticles, loaded with Cy5.5-siRNA, are apparent in the confocal images, as the diffuse transfer of the DiI lipid stain (from the lipid coating of the nanoparticle) and the 5FAM label (attached to the iRGD targeting peptide) to the cells
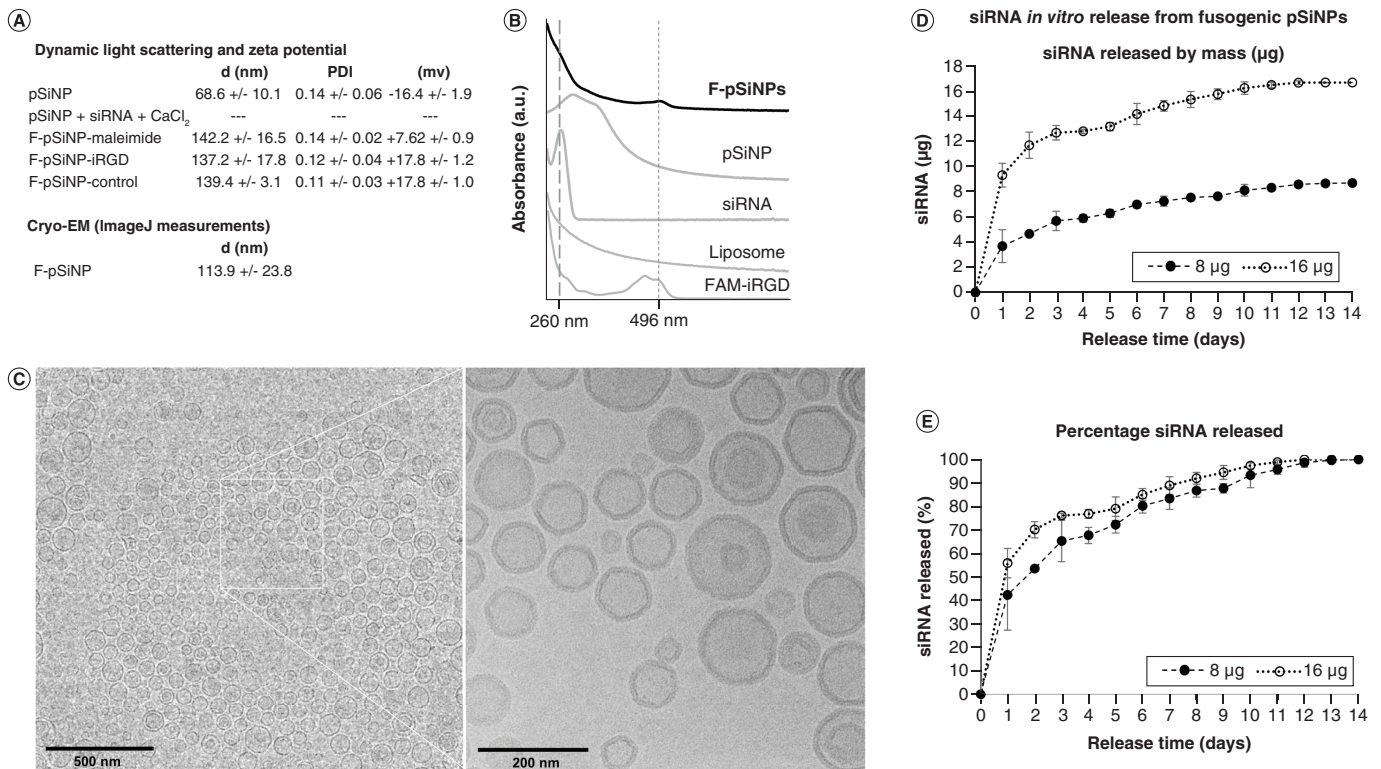
Figure 2.   Characterization of fusogenic porous silicon nanoparticles. (A) Dynamic light scattering and zeta potentials for F-pSiNPs and intermediate stages of synthesis, and ImageJ measurements from Cryo-EM. **(B)** Absorbance spectra of F-pSiNPs and the synthesis components. **(C)** Cryo-EM images, scale bar = 500 nm and 200 nm, at 10,000 and 30,000 magnification, respectively. **(D–E)** *In vitro* release study of F-pSiNPs in PBS buffer (pH 7.4) at 37°C under constant agitation. **(D)** Temporal siRNA release curve, measured by absorbance, from two FNP samples at 1× and 2× the concentration that was used for *in vivo* injections. **(E)** Same data from **(D)** but converted to the percentage of siRNA released from each F-pSiNP formulation as a function of time.
Cryo-EM: Cryogenic electron microscopy; F-pSiNP: Fusogenic porous silicon nanoparticle; PBS: phosphate buffered saline; PDI: Polydispersity index; pSiNP: Porous silicon nanoparticle.

was observed after 20 min incubation at 37°C (Figure 3C). Evidence of whole particle uptake was also observed (Figure 3C). *In vitro* F-pSiNP function was tested by VEGF-A knockdown against free siRNA incubated with Lipofectamine 2000 and F-pSiNPs with scrambled nontargeting control peptide using a particle incubation time of 24 h with ARPE-19 cells. At 48 h, VEGF-A levels were then measured by ELISA of the ARPE-19 cell lysates. A significant reduction in VEGF-A compared with the naive control cells was measured for each condition tested: F-pSiNPs, siRNA-Lipofectamine and control peptide F-pSiNPs with p = 0.0072, 0.0441 and 0.0164, respectively (Figure 3D). *In vitro* F-pSiNP-iRGD uptake was assessed against a control peptide using particles loaded with Cy5.5-siRNA. The particles were incubated for 15 min at 37°C with ARPE-19 cells, followed by washing three times with DPBS. Uptake was measured by Cy5.5 fluorescence using flow cytometry and no statistically significant difference was measured (p = 0.4348) (Figure 3E).

To measure toxicity and inflammation, four healthy animals were injected with 50 μl of the F-pSiNP treatment containing 25 μg of siRNA in their right eye, and their fellow eye was left as a no-injection control. At weeks 2, 4, 8 and 12 post-treatment, both eyes of each animal were examined by clinically trained ophthalmologists by fundus exam, ERG to measure retinal function and imaged for retinal health by OCT. All ERG *t*-yest p-values support no difference between the treated and control eyes and no evidence of toxicity or inflammation was seen by clinical exam or OCT images (Supplementary Figures 3A–C & 4A & B).

Diffusion and uptake of the intravitreally injected iRGD-F-pSiNPs with 25 μg of siRNA were evaluated in two animals at 72 h postinjection, in DL-AAA retinal angiogenesis rabbit eyes using F-pSiNPs that included DiI or sham injection controls (Table 1 & Figure 4A–D). The particles were observed to have been taken up by transretinal cells that appear to be Müller cells and had migrated toward the outer nuclear layer (Figure 4A–C).
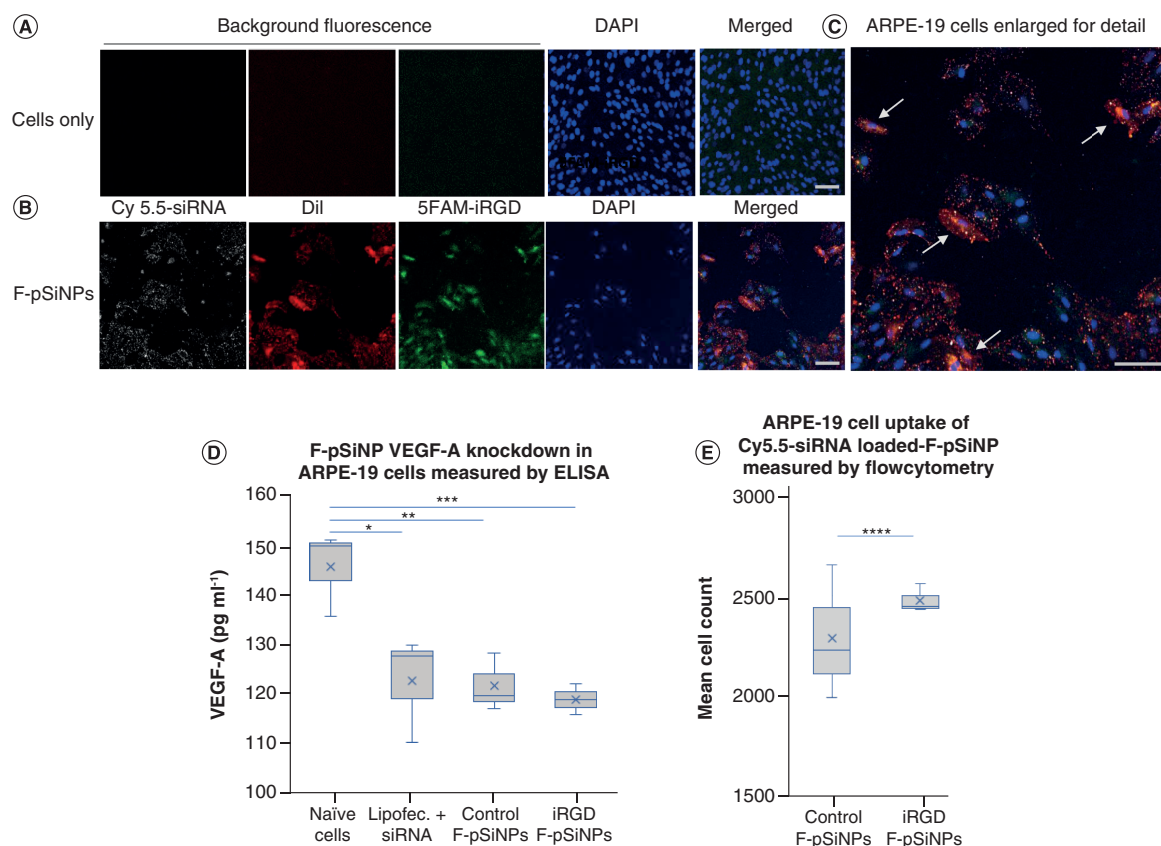
Figure 3. *In vitro* assays of human retinal pigment epithelial cells (ARPE-19) treated with iRGD-targeted fusogenic porous silicon nanoparticles. (A–C) Confocal images of the fusogenic nanoparticles loaded with Cy5.5-siRNA (grayscale), the lipophilic fluorophore DiI (red) incorporated into the fusogenic lipid coating, 5FAM (green) covalently attached to the iRGD targeting peptide and DAPI (blue) used to stain the cell nuclei. **(A)** No-nanoparticle background fluorescence control image, **(B)** ARPE-19 cells incubated with F-pSiNPs and **(C)** the **(B)** 'merged' panel enlarged for detail, with white arrows indicating regions of high fusogenic uptake. The scale bars = 100 μm. **(D)** VEGF-A ELISA data of lysed ARPE-19 cells after 24 h incubation with siRNA + lipofect., a scrambled control peptide on F-pSiNPs, or iRGD-F-pSiNPs. **(E)** The mean value flow cytometry data from iRGD-F-pSiNPs or scrambled control peptide on F-pSiNPs, each loaded with Cy5.5-siRNA. Cells were analyzed for Cy5.5 emission, and DAPI was used as a live/dead control. *$p = 0.0441$; **$p = 0.0164$; ***$p = 0.0072$, by one-way analysis of variance relative to naive cells. ****$p = 0.4348$ by Satterthwaite *t*-test.
5FAM: 5-carboxyfluorescein; DAPI: 4',6-diamidino-2-phenylindole; DiI: 1,1'-dioctadecyl-3,3,3',3'-tetramethylindocarbocyanine perchlorate; F-pSiNP: Fusogenic porous silicon nanoparticle; Lipofect.: Lipofectamine 2000.

Finally, the efficacy of the iRGD-F-pSiNP formulation was tested in the DL-AAA retinal angiogenesis rabbit model, and leakage was measured by FA imaging at 2 weeks postinjection to obtain a baseline (Table 1). Only one eye of each animal was injected with DL-AAA (80 μl 80 mM DL-AAA, pH 7.4) and the contralateral eye of each animal was injected with BSS as an injection control. By week 2, the formation of tortuous vessels and substantial vascular leakage was evident (Supplementary Figure 5A–C), characteristic of the disease model as previously described [43,44]. At week 2, 50 μl of the F-pSiNP treatment containing 25 μg of siRNA (or BSS control) was injected into the DL-AAA disease model eyes. This dose, equivalent to 10 μg kg^{-1} siRNA was selected based on the bevasiranib siRNA concentration used in the AMD clinical trial [55] which equates to 25 μg in a 50 μl injection volume for a 2.5 kg rabbit. The treatment and control animals were imaged by FA every 2 weeks thereafter to monitor changes in vascular leakage. All study animals were also evaluated by ophthalmologists by indirect fundus exams before each imaging session for toxicity and inflammation. No evidence of ocular inflammation attributed to the nanoparticles was observed.

The animals were followed for 12 weeks post-treatment (Figure 5A & B). The images were montaged and measured using ImageJ for leakage area and leakage intensity (the average pixel intensity within the measurement
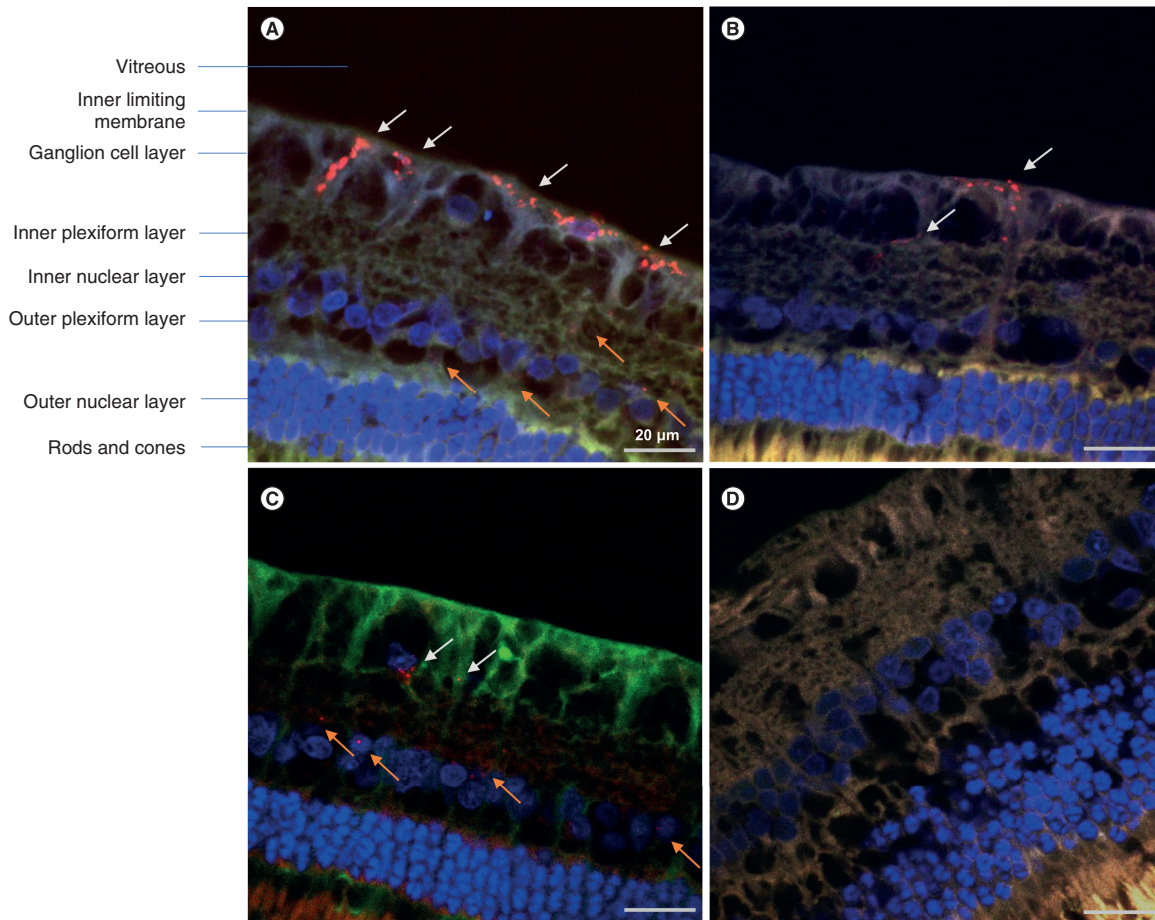
Figure 4.   Confocal microscope images of rabbit eye histology sections 72 h post-treatment with iRGD-targeted fusogenic porous silicon nanoparticles. (A & B) Fusogenic lipid-coated porous silicon nanoparticles loaded with the lipophilic fluorophore 1,1′-dioctadecyl-3,3,3′,3′-tetramethylindocarbocyanine perchlorate
(red), 4′,6-diamidino-2-phenylindole (DAPI) stained with DAPI nuclear stain (blue) and tissue autofluorescence (gray).
(C) Müller cells are stained with rabbit antiglutamine synthetase (green) and **(D)** sham treatment. The white arrows indicate particles that appear to be taken up by Müller cells. The orange arrows indicate particles transported toward the outer nuclear layer. Scale bars = 20 μm.

area) at each time point by two ophthalmologists (Figures 5A–B & 6A–C). The identities of the montaged images were masked from the ophthalmologists to avoid bias. The relative intensity of each image was corrected to the intensity of the optic nerve and compared with baseline using the equations in Figure 6C. The results showed a statistically significant difference in fluorescein leakage over time for treated versus control animals (p = 0.0137; n = 5 treated and n = 4 sham) (Figure 6D–E). Both the degree of tortuosity and the number of IrMAs were evaluated, and while both tortuosity and IrMAs were observed in both the BSS and treated eyes, no statistically significant change was seen over the course of the 12-week treatment (Supplementary Figure 6A & B). The effect of the F-pSiNP treatment on VEGF-A expression was assessed by VEGF-A ELISA performed on the vitreous humor 1, 4 and 12 weeks after treatment (Table 1 & Figure 7). Significant reduction in the concentration of VEGF-A was observed in the vitreous fluid of treated eyes at 1-, 4- and 12-week post-treatment (p = 0.0348, p = 0.0014 and p = 0.0262, respectively, n = 3 or 4), compared with each animal's untreated, naive fellow eye. This animal model has been shown to produce elevated levels of VEGF-A in both the vitreous and aqueous compartments [44]. However, the VEGF-A concentrations measured in the aqueous humor were at or near the limit of detection of the ELISA assay (data not shown), so no comment can be made on the difference in VEGF-A expression in the aqueous compartment for treated versus untreated eyes.
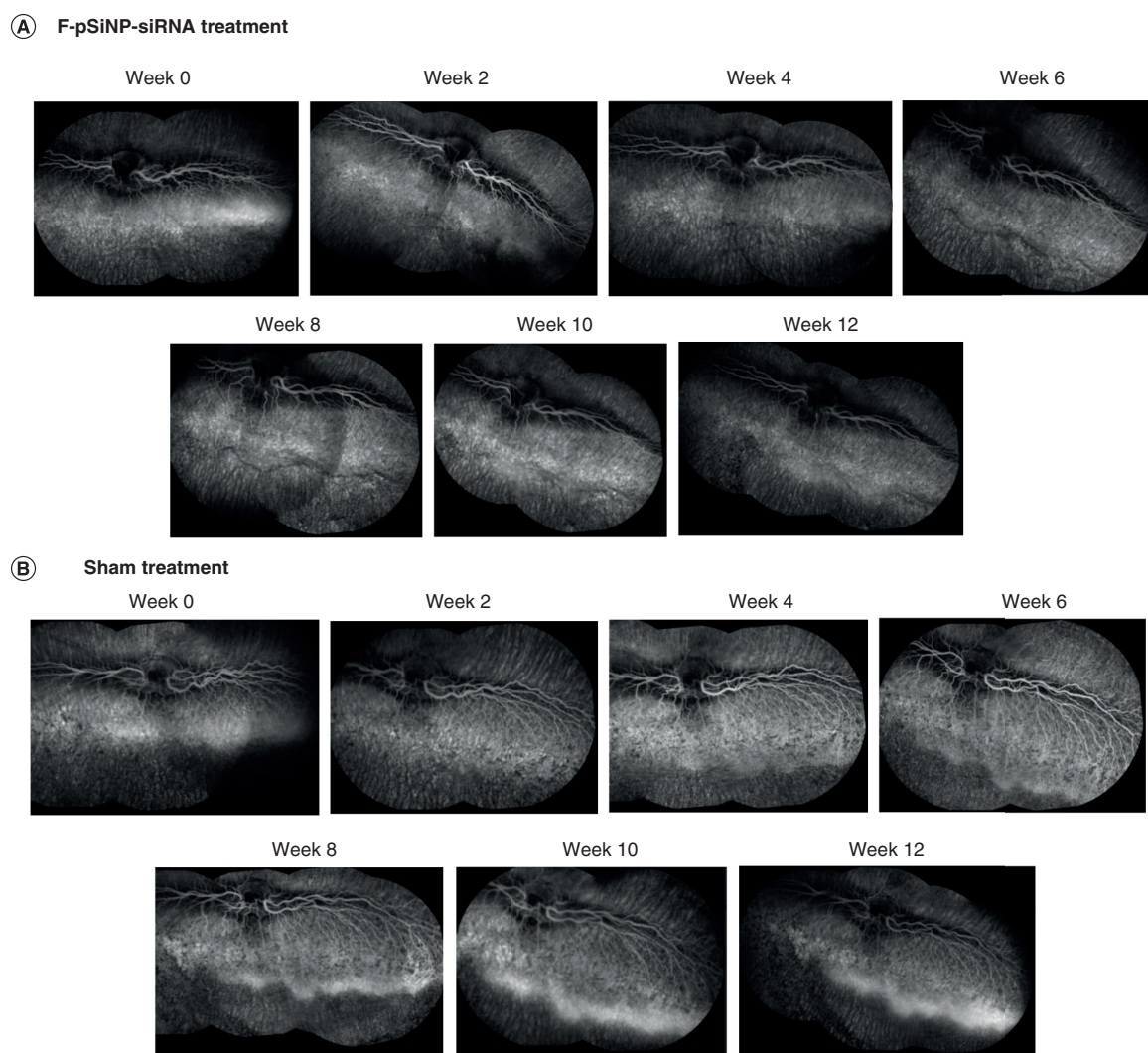
Figure 5.   Representative images of fluorescein angiography leakage post-DL-alpha aminoadipic acid injection. (A) F-pSiNP-siRNA treated eye. **(B)** Sham balanced salt solution-treated eye. Week 0 is 2 weeks post-DL-alpha aminoadipic acid injection and is used for the baseline measure of leakage. Week 0 is the day of the nanoparticle treatment or sham injection. Animals were imaged every 2 weeks for 12 consecutive weeks post-treatment.
F-pSiNP: Fusogenic porous silicon nanoparticle.

Discussion

The goal of this project was to demonstrate the possibility of transforming the current standard of care in the treatment of PDR and DME by using a targeted VEGF-siRNA nanoparticle therapy that might be able to inhibit retinal neovascularization for substantially longer periods of time than is achieved with the current standard of care. By shutting down VEGF production, rather than binding it after secretion, this approach offers the potential for more complete inhibition of disease progression. Other groups have recently demonstrated similar approaches to intravitreally injected nanoparticle siRNA therapeutics. Huang and Chau evaluated liposome nanoparticles containing nonspecific FAM-siRNA for differences in retinal uptake associated with lipid surface charge and found nanoparticles with +35 mV zeta potential showed the optimal uptake in the mouse retina [56]. Nanoparticles containing VEGFR-1 siRNA complexed with hyaluronic acid and protamine, followed by lipid coating, were found to protect against choroidal neovascularization in laser-induced choroidal neovascularization (L-CNV) rat model [57]. Another group linked several VEGF-A siRNA strands together using 5′ terminal disulfide bonds and condensed the poly-siRNA constructs into nanoparticles using polyethylene amine [58]. Their work demonstrated a reduction in choroidal neovascularization size using a mouse model of L-CNV [58]. It should be noted here that
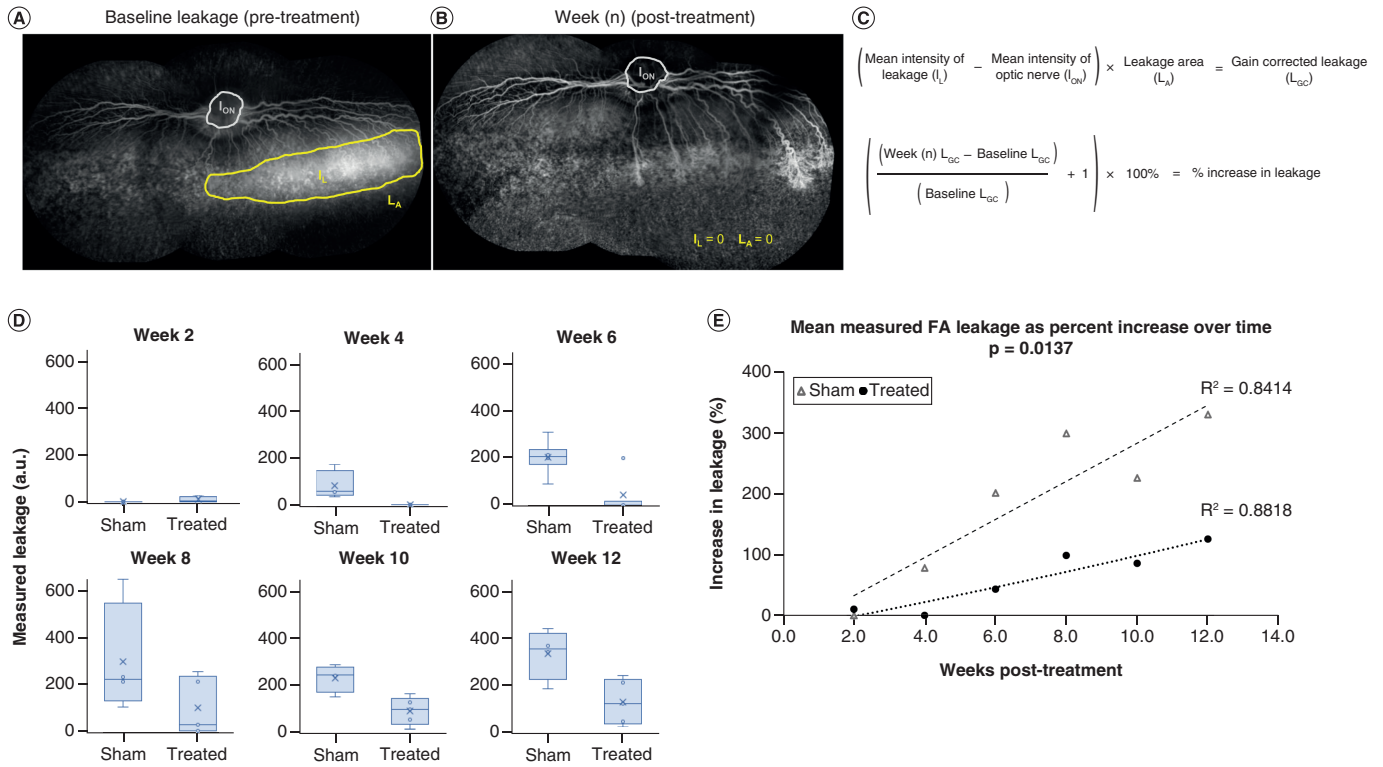
Figure 6. **Mid-phase fluorescein angiography data for rabbit eyes injected with DL-α aminoadipic acid and treated with fusogenic porous silicon nanoparticles or sham treatment. (A)** Representative image of montaged FA leakage at 2 weeks postdisease induction (baseline) and **(B)** number of weeks (n) post-treatment. Leakage area (L_A) is circled in yellow, the intensity of leakage (I_L) within the circle, and the intensity of the optic nerve (I_{ON}) within the grey circle. **(C)** Mathematical relationships used to quantify leakage from FA images and analyzed with ImageJ for the regions of interest as shown in **(A)** and **(B)**, adjusted for gain using the region of the optic nerve within each montage, resulting in gain-corrected leakage (L_{GC}). **(D)** General linear model (GLM) repeated measures analysis of variance box plots for measured fluorescein angiography leakage data. **(E)** Plot of the increase in the mean percent of corrected leakage from baseline versus weeks post-treatment showing fusogenic porous silicon nanoparticle-treated animals (circles) and sham balanced salt solution-treated animals (triangles), n = 5 treated and n = 4 sham, p = 0.0137 by general linear model repeated measures analysis of variance. FA: Fluorescein angiography.

other researchers demonstrated that extracellular siRNA can indiscriminately arrest lesion formation in murine L-CNV models [18,19]. While the above 'soft' delivery systems based on liposomal or polymeric constituents have shown promise, the present work evaluated if a delivery system based on a solid nanoparticle component might be engineered to more effectively enhance intracellular delivery and extend the duration of action of the siRNA therapeutic.

While this work explores a new use of iRGD targeting peptide technology for the delivery of nanoparticles to the interior of retinal cells, it relies on key prior work that explored the concept of directing nanoparticles to ocular tissues, either by intravitreal injection or by topical administration. Cyclic-RGD, the predecessor of iRGD, was conjugated to PEG-poly(lactic-co-glycolic acid) (PEG-PLGA)-dexamethasone grafted with polyethylene amine and the anti-VEGF antibody bevacizumab [59]. These particles were tested by intravitreal injection in a rabbit model of L-CNV and were shown to be more efficacious than nontargeted particles [59]. Doxorubicin was encapsulated within a liposome and targeted to the tyrosine kinase receptor EphA2 that is expressed on tumor neovascular cells as a potential treatment for choroidal neovascularization [60]. That work employed the YSA peptide conjugated to the surface of the nanoparticle, and intravitreal injection of the construct reduced neovascularization in a rat model of L-CNV [60]. TAT peptide-linked PLGA particles were used to deliver the anti-inflammatory drug flurbiprofen to a rabbit model of anterior chamber inflammation and demonstrated corneal penetration and efficacy [61]. Chu *et al.* further demonstrated a topical corneal application of iRGD-TAT PLGA nanoparticles had some success targeting choroidal neovascularization, most likely by periocular absorption [62]. These studies taken as a whole support the
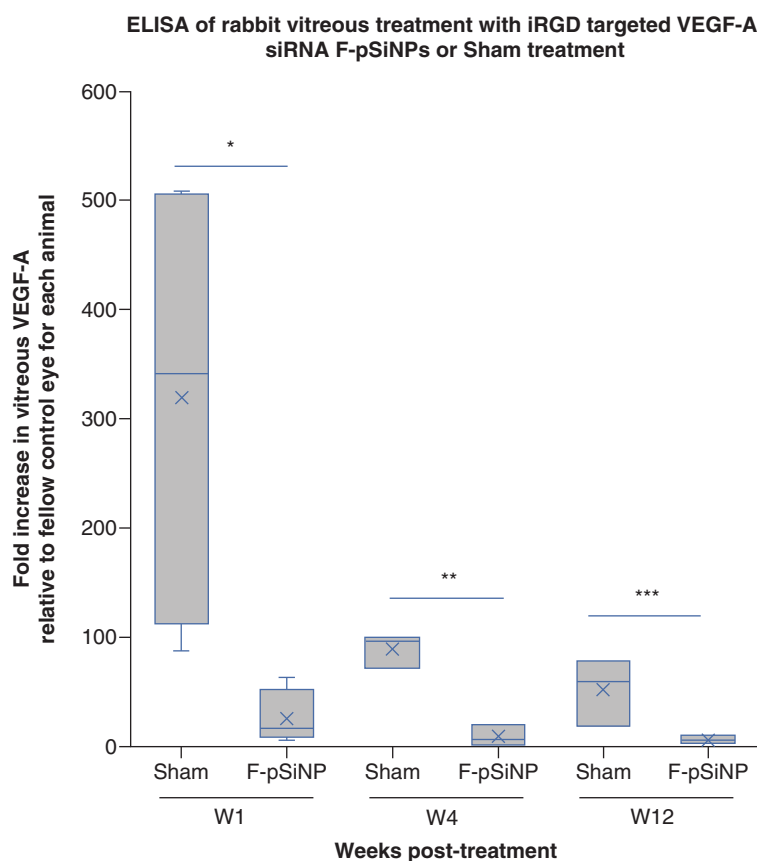
ELISA of rabbit vitreous treatment with iRGD targeted VEGF-A siRNA F-pSiNPs or Sham treatment

Figure 7.   Post-mortem ELISA of rabbit vitreous showing the fold increase in VEGF-A concentration in DL-a-aminoadipic acid diseased eyes compared with the fellow eye of the same animal. The plot compares sham- and F-pSiNP-treated animals, sacrificed at each time point of 1-, 4- and 12-weeks post-treatment (n = 3 or 4 for each group).
*p = 0.0348; **p = 0.0014; ***p = 0.0262.
F-pSiNP: Fusogenic porous silicon nanoparticle.

rationale for the focus of the present work: to use iRGD-targeted nanoparticles to deliver siRNA targeting retinal angiogenesis by intravitreal administration.

Cryo-EM showed that the F-pSiNPs take on a spherical liposome-like morphology (Figure 2C) with overall dimensions comparable to liposomes (100–200 nm). While the core pSiNPs can be easily imaged by TEM (Supplementary Figure 1A & B), once cryogenically frozen, these same particles could not be found. To address this, we used scanning transmission electron energy loss to measure the elemental composition within the liposomes (Supplementary Figure 2). The control pSiNP silicon dioxide spectra were taken from a larger micron-sized empty porous silicon precursor particle, used to make the pSiNPs. The liposome-encapsulated particles were scanned for the same spectral signatures. Based on our scanning area we estimate ∼5% of the lipid-coated particles had a measurable signal, where the $L_{2,3}$ edge peaks could be assigned based on previously published x-ray crystallographic studies [53]. The measured signal intensities were greatly reduced in comparison to the control pSi. We hypothesize this is because the nano-sized core particles have less silicon dioxide by mass than the micron-sized particles, and some of the silicon dioxide in the nanoparticles has been converted to calcium silicate. Particles with no electron energy loss signal likely had little to no pSi present. However, a large fraction of particles with Cy5.5-siRNA fluorescence aligns with both the lipid DiI and 5FAM-iRGD fluorescence from confocal microscopy (Figure 3A–C). These data taken as a whole suggest that some liposomes were 'empty', containing only free siRNA, and a smaller fraction of the liposomes contained the intact pSiNP-siRNA construct. We believe the primary reason for this result is that the extrusion conditions used to encapsulate the siRNA-loaded pSiNPs resulted in substantial dissolution of the pSiNP-siRNA construct that released the siRNA payload into the extrusion solution; the free siRNA was then encapsulated into the 'empty' liposomes during the extrusion process. The initial mass loading of siRNA in the nanoparticles was also higher than typical polymer or liposomal formulations due to the beneficial electrostatics and aqueous chemistry of the calcium-silicate system [35], and the release kinetics *in vitro* resulted in an initial burst of approximately half of the siRNA payload, followed by slow release for an additional 10–12 days (Figure 2D). For the ophthalmic applications of interest, release over several weeks to months might be more appropriate. Refining the lipid coating methods to maximize the number of liposomes that contain pSiNP-siRNA

nanoparticles, extending the release of these formulations over longer periods of time and tailoring the temporal release profile are future goals.

Another avenue of pursuit for extending therapeutic action into timescales of several months is in the design of the nucleic acid therapeutic. While an advantage of RNA-based gene modification is that it provides a more reversible effect than DNA, restriction-enzyme or genome editing-based approaches, the relatively transient nature of siRNA technology suggests that it may not provide the long-term VEGF suppression desired for the treatment of diseases such as macular degeneration, PDR or DME. Indeed, this likely was a contributor to the clinical failures of the early bevasiranib siRNA constructs used to treat AMD [63]. In subsequent years, RNA interference companies have developed chemically modified RNAs for their drugs, with modifications of multiple types (and at multiple sites) along the RNA strand to minimize immune stimulation, reduce off-target cleavage and generally increase efficacy and duration of action. For example, the FDA-approved GIVLAARI™ and OXLUMO™ of Alnylam Pharmaceuticals both contain 44 ribose and 6 phosphate backbone modifications each. These recent entries show that substantially increased stability and longer residence times can be achieved by optimizing the backbone chemistry [20]; sustained *in vivo* efficacy for as long as 6 months has been demonstrated [21]. In the present work, the first two 5′ nucleosides of the antisense strand contained 2′ methoxy modifications in order to inhibit exonuclease cleavage and increase *in vivo* stability, which presumably contributed to the relatively long-lived activity observed for the single injection. Prevention of abnormal VEGF production using long-acting siRNA would prevent PDR. This has been shown in trials of ranibizumab and aflibercept in eyes with advanced nonproliferative retinopathy [11,64]. Frequent intravitreal injections in such eyes might not be practical but a long-acting therapy to prevent VEGF production could be possible with our nanoparticles. The introduction of additional RNA modifications is an avenue for future work that might further enhance stability and extend the activity of the formulation.

Confocal microscopy demonstrated the rapid fusion of the F-pSiNPs with one potential target cell line of interest *in vitro* (Figure 3A–C). The fluorescent markers on the liposomal coating (Dil) and on the iRGD targeting peptide (5FAM) indicated successful fusion with ARPE-19 cells; both the Dil and the FAM labels were seen predominately localized in what appear to be the cell membranes, as indicated by white arrows in Figure 3C. This is consistent with the established mechanism of uptake of this nanoparticle composition, wherein the lipid coating on the nanoparticle fuses to the cell membrane and is shed from the exterior of the pSiNP, resulting in the insertion of a mostly 'bare' pSiNP into the cytosol [35]. A significant reduction in VEGF-A expression was also measured by ELISA of the cell lysates and compared with the effects of siRNA-Lipofectamine and a scrambled control peptide (Figure 3D). Here all three methods of siRNA delivery yielded a comparable reduction in VEGF-A after 24 h incubation with cells (Figure 3D), demonstrating that the siRNA remained functional after loading, and the F-pSiNPs were comparable to the transfection gold standard Lipofectamine *in vitro*. The role of iRGD in the *in vitro* uptake was also measured with flow cytometry and compared with the control peptide. No statistically significant difference in uptake of Cy5.5-siRNA was measured after 15 min of incubation with the cells (p = 0.4348) (Figure 3E). Both formulations had similar diameters and almost identical zeta potentials measured by DLS (Figure 2A). These data suggest that the surface charge and fusogenic properties of the particles are likely a primary mechanism for cell adhesion and uptake *in vitro* with this cell line. Additional work is needed to determine the detailed role of iRGD *in vivo*.

In vivo, 72 h after intravitreal injection in rabbit eyes, evidence of the lipid dye can be seen at the inner limiting membrane, within transretinal cells and at the inner nuclear layer (Figure 4A–C), suggesting that at least some of the components, and likely some of the intact lipid-coated nanoparticles, are transported deeper into the retina. Further study is needed to estimate regional localization and to quantitate these particle observations; however, this rapid diffusion and uptake would reduce the possibility of disturbance of vision from the presence of particles in the vitreous.

Ophthalmologists from our group evaluated the F-pSiNPs for *in vivo* tolerability by indirect fundus exam, clinical exam, ERG and OCT after nanoparticle injection compared with each animal's control fellow eye in healthy, no disease animals (Supplementary Figures 3A–C & 4A & B). The treated eyes showed no evidence of toxicity or inflammation attributed to the presence of the nanoparticles, and no statistically significant difference in retinal function by ERG. These exams continued over the course of a 12-week period to allow comparison with the animal groups used in the efficacy study. This biocompatibility is in agreement with our previous studies using intravitreal injections of microparticles of porous silicon [22–25,65].

The *in vivo* rabbit model used for PDR and DME exhibited retinal neovascularization and vascular leakage indicative of pathologic vessel growth associated with these diseases. The Müller cell toxin DL-AAA was injected intravitreally and has been shown to induce the pathology of the model in the first 2 weeks [43–45], which was

supported by the present findings (Supplementary Figure 5A–C & Figure 5A–B). Müller glial cells are specific to the retina and are responsible for protecting neurons, maintaining homeostasis and neuronal metabolic support [46]. They have been shown to undergo gliosis in PDR and in doing so contribute to the progression of the disease by the release of angiogenic cytokines such as VEGF [46,47]. VEGF in turn promotes neovascular growth and induces vascular leakage [2,3]. A single injection of DL-AAA exhibited a retinal neovascular pathology in rabbits from 2 to 65 weeks postinjection [43,44]. Prior studies with this model have shown that injection of the anti-VEGF drug aflibercept (Eylea®, 0.5 mg dose) was able to temporarily stop vascular leakage for 8 weeks, after which time recurrence of vascular leakage was observed [43,44]. Those results demonstrated both the association of VEGF-A with vascular leakage and the stability of the pathology. Our data exhibited a comparable performance resulting in an inhibition of leakage for up to 12 weeks (Figure 6D–E). These data correlated well with post-mortem VEGF-A vitreous ELISA analyses demonstrating a significant reduction in VEGF-A at both 1, 4 and 12 weeks after F-pSiNP treatment relative to untreated DL-AAA animals at the same time points (Figure 7) and resulted in an 8.4-fold decrease in VEGF-A for the treated animals over sham control animals at 12 weeks (p = 0.0262; n = 3–4 each).

It should be noted that in this disease model we observed a refractory period of leakage at week 4 after DL-AAA injection (corresponding to week 2 after treatment) in all study animals, including sham controls (Figure 5A & B). This was also evident in the high level of variability in VEGF-A expression from the ELISA data of the sham-treated animals occurring at week 1, which was significantly reduced by week 4 (Figure 7). This refractory period indicates a change in retinal response to the DL-AAA that requires further investigation. In addition, the dose of 80 μl of 80 mM DL-AAA resulted in substantial incidences of retinal detachment (>50%) in the animals, a sign of severe disease that eliminates the utility of FA imaging. These animals with detached retinas were excluded from the FA imaging studies because no leakage could be measured, but they were used in the vitreous ELISA studies (reflected in Table 1). This incidence of detachment was substantially higher than the previously reported percentage of animals (20%) that experienced these adverse events [43]. Because the VEGF-A molecular analysis was performed using these animals with severe disease (i.e., those with retinal detachments), it is likely that the levels of VEGF-A reported in this work are an upper estimate, and VEGF-A expression in the animals used to quantify leakage (FA imaging) were likely lower. Animal welfare concerns precluded running of scrambled siRNA or nontargeting controls on this model. Future work will include evaluating the model at lower doses of DL-AAA in order to minimize adverse retinal detachment events. While the present work showed that iRGD-targeted F-pSiNPs are highly effective at suppressing vascular leakage, establishing the overall feasibility of the approach, our *in vitro* data did not show a statistically significant difference in particle uptake attributed to the targeting peptide. The questions of whether or not the iRGD targeting group is essential, and which cells can (or should) be targeted were not addressed.

Conclusion

This study was the first to attempt utilizing fusogenic pSiNPs-iRGD technology for the intraretinal delivery of VEGF-siRNA. The study established the feasibility of using a combination of a solid, but resorbable, nanoparticle with cellular targeting and penetration innovations to overcome prior limitations of nucleic acid therapeutics for knocking down VEGF expression. The positive results in reducing vascular leakage in the rabbit model over a 3-month period indicate that this is a promising approach to treating debilitating eye diseases such as macular degeneration, PDR or DME.

Summary points

- The chronic pathology of proliferative diabetic retinopathy and diabetic macular edema requires a protracted level of therapeutic intervention to maintain remission.
- Due to the high turnover of antibody therapeutics in the vitreous, repeated monthly injections are required which run the risk of intraocular inflammation, infection and ocular hemorrhage. Repeated high concentration injections of anti-VEGF can result in retinal geographic atrophy and adverse reactions from systemic circulation.
- Using targeted siRNA as an alternative therapeutic approach has the potential to extend efficacy by specifically, and catalytically, knocking out the intracellular pathogenic protein synthesis machinery, rather than only sequestering individual excreted proteins.
- Porous silicon nanoparticles loaded with VEGF-A siRNA were coated with a fusogenic lipid composition (F-pSiNPs) which incorporated the targeting and internalization peptide iRGD that homes neovascular integrins.
- The F-pSiNPs were evaluated by intravitreal injection in the DL-α-aminoadipic acid rabbit model of retinal neovascularization. Efficacy was measured by a reduction of leakage using fluorescein angiography as compared with sham controls and confirmed with vitreous VEGF-A ELISA and histology.
- A statistically significant reduction in rabbit ocular fluorescein angiography leakage was observed for treated diseased eyes as compared with the control sham eyes ($p = 0.0137$), which persisted for 12 weeks, as compared with 8 weeks or less, as reported by other groups testing current anti-VEGF therapies using this animal model.
- A reduction in the concentration of vitreous VEGF-A was observed for 12 weeks post-treatment. Histological sections from 72 h postinjection revealed penetration of the F-pSiNPs throughout the inner retina and up to the retinal pigment epithelium.
- F-pSiNP delivery of siRNA provides persistent knockdown of VEGF-A and reduces leakage in a rabbit model of retinal angiogenesis as a potential new intraocular therapeutic.

Ethical conduct of research

All animal studies were performed using New Zealand pigmented rabbits, which were treated in accordance with the University of California, San Diego, American Association for Laboratory Animal Science the Institutional Animal Care and Use Committee (IACUC) standards of practice, and in accordance with the Association for Research in Vision and Ophthalmology statement for the use of animals in ophthalmic and vision research.

References

Papers of special note have been highlighted as: ● of interest; ●● of considerable interest

1.   Lee R, Wong TY, Sabanayagam C. Epidemiology of diabetic retinopathy, diabetic macular edema and related vision loss. *Eye Vis. (Lond.)* 2, 17 (2015).

2.   Cai J, Boulton M. The pathogenesis of diabetic retinopathy: old concepts and new questions. *Eye (Lond.)* 16(3), 242–260 (2002).

3.   Campochiaro PA. Ocular neovascularization. *J. Mol. Med. (Berl.)* 91(3), 311–321 (2013).

4.   Rosenfeld PJ, Windsor MA, Feuer WJ *et al.* Estimating medicare and patient savings from the use of bevacizumab for the treatment of exudative age-related macular degeneration. *Am. J. Ophthalmol.* 191, 135–139 (2018).

5.   Writing Committee for the Diabetic Retinopathy Clinical Research Network, Gross JG, Glassman AR *et al.* Panretinal photocoagulation vs intravitreous ranibizumab for proliferative diabetic retinopathy: a randomized clinical trial. *JAMA* 314(20), 2137–2146 (2015).

6.   Mitchell P, Bandello F, Schmidt-Erfurth U *et al.* The RESTORE study: ranibizumab monotherapy or combined with laser versus laser monotherapy for diabetic macular edema. *Ophthalmology* 118(4), 615–625 (2011).

7.   Mitchell P, Massin P, Bressler S *et al.* Three-year patient-reported visual function outcomes in diabetic macular edema managed with ranibizumab: the RESTORE extension study. *Curr. Med. Res. Opin.* 31(11), 1967–1975 (2015).

8.   Heier JS, Korobelnik JF, Brown DM *et al.* Intravitreal aflibercept for diabetic macular edema: 148-week results from the VISTA and VIVID studies. *Ophthalmology* 123(11), 2376–2385 (2016).

9.   Heng LZ, Comyn O, Peto T *et al.* Diabetic retinopathy: pathogenesis, clinical grading, management and future developments. *Diabet. Med.* 30(6), 640–650 (2013).

10.   Singer MA, Awh CC, Sadda S *et al.* HORIZON: an open-label extension trial of ranibizumab for choroidal neovascularization secondary to age-related macular degeneration. *Ophthalmology* 119(6), 1175–1183 (2012).

11.   Rofagha S, Bhisitkul RB, Boyer DS, Sadda SR, Zhang K, Group S-US. Seven-year outcomes in ranibizumab-treated patients in ANCHOR, MARINA, and HORIZON: a multicenter cohort study (SEVEN-UP). *Ophthalmology* 120(11), 2292–2299 (2013).

12.   Falavarjani KG, Nguyen QD. Adverse events and complications associated with intravitreal injection of anti-VEGF agents: a review of literature. *Eye (Lond.)* 27(7), 787–794 (2013).

13.   Semeraro F, Morescalchi F, Parmeggiani F, Arcidiacono B, Costagliola C. Systemic adverse drug reactions secondary to anti-VEGF intravitreal injection in patients with neovascular age-related macular degeneration. *Curr. Vasc. Pharmacol.* 9(5), 629–646 (2011).

14.   Bressler NM, Beaulieu WT, Maguire MG *et al.* Early response to anti-vascular endothelial growth factor and two-year outcomes among eyes with diabetic macular edema in Protocol T. *Am. J. Ophthalmol.* 195, 93–100 (2018).

15.   Zhao Y, Singh RP. The role of anti-vascular endothelial growth factor (anti-VEGF) in the management of proliferative diabetic retinopathy. *Drugs Context* 7, 212532 (2018).

16.   Ozcan G, Ozpolat B, Coleman RL, Sood AK, Lopez-Berestein G. Preclinical and clinical development of siRNA-based therapeutics. *Adv. Drug Deliv. Rev.* 87, 108–119 (2015).

17.   ClinicalTrials.gov. Safety and efficacy study evaluating the combination of Bevasiranib & Lucentis Therapy in Wet AMD (COBALT). Clinical Trial Registration: NCT00499590 (2014).

18.   Kleinman ME, Yamada K, Takeda A *et al.* Sequence- and target-independent angiogenesis suppression by siRNA via TLR3. *Nature* 452(7187), 591–597 (2008).

19.   Kleinman ME, Kaneko H, Cho WG *et al.* Short-interfering RNAs induce retinal degeneration via TLR3 and IRF3. *Mol. Ther.* 20(1), 101–108 (2012).

20.   Foster DJ, Brown CR, Shaikh S *et al.* Advanced siRNA designs further improve *in vivo* performance of GalNAc-siRNA conjugates. *Mol. Ther.* 26(3), 708–717 (2018).

21.   Hu B, Zhong L, Weng Y *et al.* Therapeutic siRNA: state of the art. *Signal Transduct. Target. Ther.* 5(1), 101 (2020).

●   **Provides a current overview of siRNA as a therapeutic.**

22.   Nieto A, Hou H, Moon SW, Sailor MJ, Freeman WR, Cheng L. Surface engineering of porous silicon microparticles for intravitreal sustained delivery of rapamycin. *Invest. Ophthalmol. Vis. Sci.* 56(2), 1070–1080 (2015).

23.   Hartmann KI, Nieto A, Wu EC *et al.* Hydrosilylated porous silicon particles function as an intravitreal drug delivery system for daunorubicin. *J. Ocul. Pharmacol. Ther.* 29(5), 493–500 (2013).

24. Kashanian S, Harding F, Irani Y *et al.* Evaluation of mesoporous silicon/polycaprolactone composites as ophthalmic implants. *Acta Biomater.* 6(9), 3566–3572 (2010).

25. Low SP, Voelcker NH, Canham LT, Williams KA. The biocompatibility of porous silicon in tissues of the eye. *Biomaterials* 30(15), 2873–2880 (2009).

26. Nieto A, Hou H, Sailor MJ, Freeman WR, Cheng L. Ocular silicon distribution and clearance following intravitreal injection of porous silicon microparticles. *Exp. Eye Res.* 116, 161–168 (2013).

27. Joo J, Kwon EJ, Kang J *et al.* Porous silicon–graphene oxide core–shell nanoparticles for targeted delivery of siRNA to the injured brain. *Nanoscale Horiz.* 1, 407–414 (2016).

28. Baran-Rachwalska P, Torabi-Pour N, Sutera FM *et al.* Topical siRNA delivery to the cornea and anterior eye by hybrid silicon-lipid nanoparticles. *J. Control. Rel.* 326, 192–202 (2020).

29. Tong WY, Alnakhli M, Bhardwaj R *et al.* Delivery of siRNA *in vitro* and *in vivo* using PEI-capped porous silicon nanoparticles to silence MRP1 and inhibit proliferation in glioblastoma. *J. Nanobiotechnol.* 16, 38 (2018).

30. Kafshgari MH, Alnakhli M, Delalat B *et al.* Small interfering RNA delivery by polyethylenimine-functionalised porous silicon nanoparticles. *Biomater. Sci.* 3(12), 1555–1565 (2015).

31. Zhang MZ, Xu R, Xia XJ *et al.* Polycation-functionalized nanoporous silicon particles for gene silencing on breast cancer cells. *Biomaterials* 35(1), 423–431 (2014).

32. Wan Y, Apostolou S, Dronov R, Kuss B, Voelcker NH. Cancer-targeting siRNA delivery from porous silicon nanoparticles. *Nanomedicine* 9(15), 2309–2321 (2014).

33. Kang J, Joo J, Kwon EJ *et al.* Self-sealing porous silicon–calcium silicate core–shell nanoparticles for targeted siRNA delivery to the injured brain. *Adv. Mater.* 28(36), 7962–7969 (2016).

•• **Provides data for the discovery and characterization of calcium silicate siRNA loading into porous silicon nanoparticles and their *in vivo* application.**

34. Kim B, Pang HB, Kang J, Park JH, Ruoslahti E, Sailor MJ. Immunogene therapy with fusogenic nanoparticles modulates macrophage response to *Staphylococcus aureus*. *Nat. Commun.* 9(1), 1969 (2018).

35. Kim B, Sun S, Varner JA, Howell SB, Ruoslahti E, Sailor MJ. Securing the payload, finding the cell, and avoiding the endosome: peptide-targeted, fusogenic porous silicon nanoparticles for delivery of siRNA. *Adv. Mater.* 31(35), e1902952 (2019).

•• **Explores the application of peptide targeted fusogenic lipid coatings to porous silicon nanoparticles.**

36. Torchilin VP. Recent advances with liposomes as pharmaceutical carriers. *Nat. Rev. Drug Discov.* 4(2), 145–160 (2005).

37. Teesalu T, Sugahara KN, Ruoslahti E. Tumor-penetrating peptides. *Front. Oncol.* 3, 216 (2013).

38. Ruoslahti E. Peptides as targeting elements and tissue penetration devices for nanoparticles. *Adv. Mater.* 24(28), 3747–3756 (2012).

• **Ruoslahti is a professor emeritus and leader in the field of targeting peptide discovery. Here Rouslahti provides a review of peptide targeting of nanoparticles.**

39. Ruoslahti E. Tumor penetrating peptides for improved drug delivery. *Adv. Drug Deliv. Rev.* 110–111 (2017).

40. Sugahara KN, Teesalu T, Karmali PP *et al.* Tissue-penetrating delivery of compounds and nanoparticles into tumors. *Cancer Cell* 16(6), 510–520 (2009).

41. Friedlander M, Theesfeld CL, Sugita M *et al.* Involvement of integrins alpha v beta 3 and alpha v beta 5 in ocular neovascular diseases. *Proc. Natl Acad. Sci. USA* 93(18), 9764–9769 (1996).

42. Fernandez-Robredo P, Selvam S, Powner MB, Sim DA, Fruttiger M. Neuropilin 1 involvement in choroidal and retinal neovascularisation. *PLOS ONE* 12(1), e0169865 (2017).

43. Cao J, Macpherson TC, Iglesias BV *et al.* Aflibercept action in a rabbit model of chronic retinal neovascularization: reversible inhibition of pathologic leakage with dose-dependent duration. *Invest. Ophthalmol. Vis. Sci.* 59(2), 1033–1044 (2018).

•• **Demonstrates the DL-AAA animal model for retinal neovascular leakage used in this work and includes efficacy data using the current gold-standard antibody drug aflibercept.**

44. Li Y, Busoy JM, Zaman BAA *et al.* A novel model of persistent retinal neovascularization for the development of sustained anti-VEGF therapies. *Exp. Eye Res.* 174, 98–106 (2018).

45. Shen W, Li S, Chung SH, Gillies MC. Retinal vascular changes after glial disruption in rats. *J. Neurosci. Res.* 88(7), 1485–1499 (2010).

46. Bringmann A, Wiedemann P. Müller glial cells in retinal disease. *Ophthalmologica* 227(1), 1–19 (2012).

47. Fletcher EL, Phipps JA, Ward MM, Puthussery T, Wilkinson-Berka JL. Neuronal and glial cell abnormality as predictors of progression of diabetic retinopathy. *Curr. Pharm. Design* 13(26), 2699–2712 (2007).

48. Fu YC, Xin ZM. Inhibited corneal neovascularization in rabbits following corneal alkali burn by double-target interference for VEGF and HIF-1alpha. *Biosci. Rep.* 39(1), (2019).

49. Cheng LY, Hostetler KY, Chaidhawangul S *et al.* Intravitreal toxicology and duration of efficacy of a novel antiviral lipid prodrug of ganciclovir in liposome formulation. *Invest. Ophthamol. Vis. Sci.* 41(6), 1523–1532 (2000).

50. Schneider CA, Rasband WS, Eliceiri KW. NIH Image to ImageJ: 25 years of image analysis. *Nat. Methods* 9(7), 671–675 (2012).

51. Sailor MJ, Wu EC. Photoluminescence-based sensing with porous silicon films, microparticles, and nanoparticles. *Adv. Funct. Mater.* 19(20), 3195–3208 (2009).

52. Qin ZT, Joo J, Gu L, Sailor MJ. Size control of porous silicon nanoparticles by electrochemical perforation etching. *Part. Part. Syst. Char.* 31(2), 252–256 (2014).

53. Li D, Bancroft GM, Kasrai M *et al.* X-ray-absorption spectroscopy of silicon dioxide (SiO$_2$) polymorphs – the structural characterization of opal. *Am. Mineral.* 79(7-8), 622–632 (1994).

54. Bantseev V, Miller PE, Bentley E *et al.* Determination of a no-observable effect level for endotoxin following a single intravitreal administration to Dutch belted rabbits. *Invest. Ophthalmol. Vis. Sci.* 58(3), 1545–1552 (2017).

55. Garba AO, Mousa SA. Bevasiranib for the treatment of wet, age-related macular degeneration. *Ophthalmol. Eye Dis.* 2, 75–83 (2010).

56. Huang XN, Chau Y. Investigating impacts of surface charge on intraocular distribution of intravitreal lipid nanoparticles. *Exp. Eye Res.* 186 (2019).

57. Liu HA, Liu YL, Ma ZZ, Wang JC, Zhang Q. A lipid nanoparticle system improves siRNA efficacy in RPE cells and a laser-induced murine CNV model. *Invest. Ophthalmol. Vis. Sci.* 52(7), 4789–4794 (2011).

58. Lee J, Ryoo NK, Han H *et al.* Anti-VEGF polysiRNA polyplex for the treatment of choroidal neovascularization. *Mol. Pharm.* 13(6), 1988–1995 (2016).

59. Liu J, Luo L, Xu F *et al.* Cyclic RGD peptide targeting coated nano drug co-delivery system for therapeutic use in age-related macular degeneration disease. *Molecules* 25(21), (2020).

60. Wang JL, Liu YL, Li Y *et al.* EphA2 targeted doxorubicin stealth liposomes as a therapy system for choroidal neovascularization in rats. *Invest. Ophthamol. Vis. Sci.* 53(11), 7348–7357 (2012).

61. Vasconcelos A, Vega E, Pérez Y, Gómara MJ, García ML, Haro I. Conjugation of cell-penetrating peptides with poly(lactic-co-glycolic acid)-polyethylene glycol nanoparticles improves ocular drug delivery. *Int. J. Nanomed.* 10, 609–631 (2015).

62. Chu Y, Chen N, Yu H *et al.* Topical ocular delivery to laser-induced choroidal neovascularization by dual internalizing RGD and TAT peptide-modified nanoparticles. *Int. J. Nanomed.* 12, 1353–1368 (2017).

63. Ehrlich R, Ciulla TA. siRNA: set for a comeback? *Retinal Physician* (2010).
https://www.retinalphysician.com/issues/2010/september-2010/sirna-set-for-a-comeback

64. Brown DM, Wykoff CC, Boyer D *et al.* Evaluation of intravitreal aflibercept for the treatment of severe nonproliferative diabetic retinopathy: results from the PANORAMA randomized clinical trial. *JAMA Ophthalmol.* 139(9), 946–955 (2021).

65. Nieto A, Hou H, Sailor MJ, Freeman WR, Cheng L. Ocular silicon distribution and clearance following intravitreal injection of porous silicon microparticles. *Exp. Eye Res.* 116, 161–168 (2013).